Numerical Study of the Shrinkage Flow Induced Macrosegregation in Continuous Casting of Steel

F. Mayer, M. Gruber-Pretzler, L. Könözsy, M. Wu, A. Ludwig

CD-Lab for Multiphase Modeling of Metallurgical Processes, Simulation and Modeling of Metallurgical Processes, Dept. Metallurgy, Univ. Leoben, A-8700, Austria

ABSTRACT: Macrosegregations in steel continuous casting can be caused by different mechanisms such as feeding flow, deformation (bulging) induced flow, thermo-solutal convection, equiaxed grain sedimentation etc. The current paper focuses on the formation of macrosegregation in the mushy zone caused by the mechanism of feeding flow. A two phase volume averaging Eulerian approach is applied to simulate the solidification of a scaled benchmark strand as well as the formation of macrosegregation. It considers the liquid melt and the columnar dendrite trunks as separate phases, whereby the morphology of the growing columnar trunks is simplified as step-wise growing cylinders. A diffusion controlled growth model is implemented for calculating the mass transfer rate during solidification. In addition, the velocity field of the melt flow is calculated by solving the corresponding momentum conservation equation. The species transport equation for the interdendritic melt is explicitly solved and the thermodynamics of the binary Fe-C system is taken into account. Considering only solidification shrinkage-induced feeding, the predicted macrosegregation pattern shows a negative center segregation rather than positive.

1. INTRODUCTION

Different flow and transport phenomena during continuous casting process cause macrosegregation. The frequently occurring macrosegregation in continuously cast slab is the centerline segregation [1-5]. Industrial practice has demonstrated that this centerline macrosegregation can be reduced by the so-called softreduction procedure: at the end of solidification, the strand is subjected to weak rolling [6-9]. Due to the complexity of the coupled flow and transport phenomena, the majority of knowledge on this topic comes from experimental trials to optimize the soft reduction parameters (e.g. the reduction position and reduction rate). This is costly. Therefore, numerical studies become a more efficient method to achieve deeper understanding to this problem [1,5,10]. Very recently, two of the present authors [11-12] have developed a three-phase volume-averaging approach for predicting macrosegregations. With this approach the motion of grains, the melt flow caused by shrinkage and thermo-solutal buoyancy, the growth of a columnar front and the columnar-to-equiaxed transition can be modeled.

In the current paper only a two phase columnar solidification is considered. The permeable mushy zone is assumed to be composed of cylindrical ‘dendrites’ with a given primary dendrite arm spacing, λ_1. Further development of the dendritic growth model especially in the mushy zone has been made. The results of the feeding induced macrosegregation forming within a solidifying strand are presented and discussed.

2. MODEL DESCRIPTION AND ASSUMPTIONS

A detailed description of the numerical model is published in [11-12]. Here a short outline of the columnar solidification model is given. The model considers two phases, one for the melt and one for the growing columnar dendrites. The conservation equations of mass, species and enthalpy for each phase are included. For the melt the momentum conservation equation is solved in addition. The columnar phase is assumed to move with a fixed velocity, namely the casting velocity (v_{cast}). The main assumptions of the model are summarized as follows:

- A linearized binary Fe-C phase diagram, i.e. a constant solute redistribution coefficient k and a constant liquidus slope m, are used.
- Columnar dendrite trunks grow from the mold wall as soon as the casting surface temperature drops below liquidus T_{L}.
- The morphology of columnar dendrite trunks is simplified as cone-shaped cylinders.

- A shell-wise growth of the cylinders is driven by diffusion.
- Mechanical interaction between the solid and the liquid in the mushy zone is calculated via Darcy's law and the Blake-Kozeny permeability approach [13-14].

In order to quantitate the macrosegregation, a mixture concentration is calculated by

$$c_{\mathrm{mix}} = \frac{c_{\mathrm{l}} \cdot f_{\mathrm{l}} \cdot \rho_{\mathrm{l}} + c_{\mathrm{s}} \cdot f_{\mathrm{s}} \cdot \rho_{\mathrm{s}}}{f_{\mathrm{l}} \cdot \rho_{\mathrm{l}} + f_{\mathrm{s}} \cdot \rho_{\mathrm{s}}} \quad . \tag{1}$$

Here, c_{l} and c_{s} stand for the concentrations, f_{l} and f_{s} for the volume fractions, ρ_{l} and ρ_{s} for the densities of the liquid and the solid.

As an improvement to the previously published multiphase solidification model [11-12], the impingement factor for the columnar growth is re-considered. The calculation of the impingement factor for hexagonal arrangement of columnar dendrites is based on geometry information. The dendrite trunk diameter, d_{c}, is calculated according to the following correlation

$$d_{\mathrm{c}} = \sqrt{\frac{\sqrt{12} \cdot f_{\mathrm{s}}}{\pi}} \cdot \lambda_{1} \quad . \tag{2}$$

Based on this expression, the maximum columnar diameter $d_{\max}$ is determined by the diameter of the dendrite trunk (Fig. 1), when no liquid is left in the cell. Since the mass transfer rate M_{lc} depends on the surface per volume it can be defined as

$$M_{\mathrm{lc}} = v_{\mathrm{R_C}} \cdot \frac{2 \cdot d_{c} \cdot \pi}{\sqrt{3} \cdot \lambda_{1}^{2}} \cdot \rho_{\mathrm{s}} \cdot f_{\mathrm{imp}} \quad . \tag{3}$$

Here, $v_{\mathrm{R_C}}$ stands for the growth velocity. As the columnar trunks will no longer be ideal cylindrical, when they start to impinge, an impingement factor (f_{imp}) was defined to consider the decrease of surface per volume with further solidification.

$$f_{\mathrm{imp}} = \begin{cases} 1 & \text{when} \quad d_{\mathrm{c}} \le \lambda_{1} \\ f_{\mathrm{l}} / f_{\mathrm{l,critic}} & \text{when} \quad d_{\mathrm{c}} > \lambda_{1} \end{cases} \quad . \tag{4}$$

Here, $f_{\mathrm{l,critic}}$ is the critical liquid volume fraction defined as

$$f_{\mathrm{l,critic}} = 1 - \frac{\pi}{2 \cdot \sqrt{3}} \quad . \tag{5}$$

In order to overcome numerical difficulties at end of solidification where numerical convergence is hard to achieve, a so called simplified-porosity-model (SPM) is implemented. At a certain amount of residual melt, $f_{\mathrm{l,SPM}}$, it became quite difficult for the feeding flow to stream through the already solidified forest of dendrites. In reality, if feeding is not possible porosity might form. We treat the formation of pores by considering the next growing solid shell as a porous phase $f_{\mathrm{s+p}}$ with an average density of $\rho_{\mathrm{s+p}}$ being equal to the liquid density (Fig. 2). With this simple approach the average density of the solid phase including the primary solid phase, $f_{\mathrm{s,prim}}$, and the newly formed porous shell is calculated by

$$\overline{\rho}_{\mathrm{s}} = \frac{f_{\mathrm{s,prim}} \cdot \rho_{\mathrm{s}} + f_{\mathrm{s+p}} \cdot \rho_{\mathrm{s+p}}}{f_{\mathrm{s,prim}} + f_{\mathrm{s+p}}} \quad . \tag{6}$$

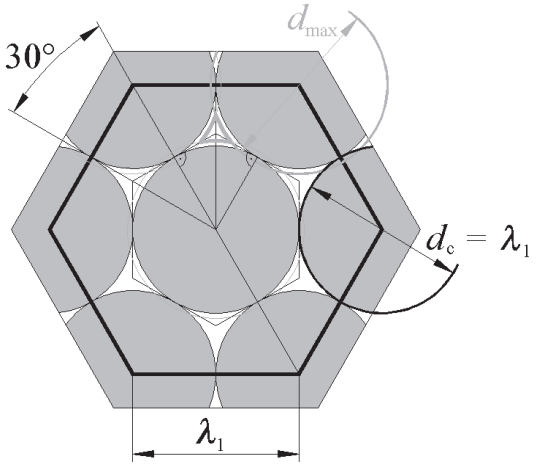

Fig. 1: Sketch of hexagonal arrangement.

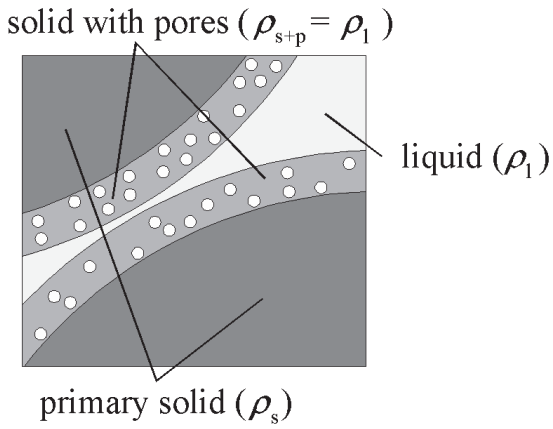

Fig. 2: Basic idea to treat the pore formation in a growing shell with a solid average density.

3. PROBLEM DESCRIPTION

For the presented calculation the properties of a binary steel Fe-0.18wt.%C were used. The solidification simulations were performed with the software FLUENT in combination with the model outlined above by user defined subroutines [11-14]. For the geometry the scaled benchmark shown in Fig. 3 has been chosen. The casting velocity of v_{cast} = 3.5 mm/s = 12.6 m/h and a casting temperature of T_0 = 1791 K were applied for the continuous casting process. A 2D-symmetrical simulation was made. Fig. 3 schematically shows the calculation domain, where (①) indicates the position of a pressure inlet, (②) shows a heat transfer coefficient (HTC) boundary with h = 235 W/m²/K and T_{wall} = 325 K, and (③) indicates the location of the outlet. Here, a constant casting velocity is taken as outlet boundary condition. (④) labels the location of the symmetry plane. The wall (②) is assumed to move with the casting velocity. Therefore, a non-slip condition for the wall boundary is applied. The calculation domain is discritizied with 245 760 cells. In this work only steady state results are presented.

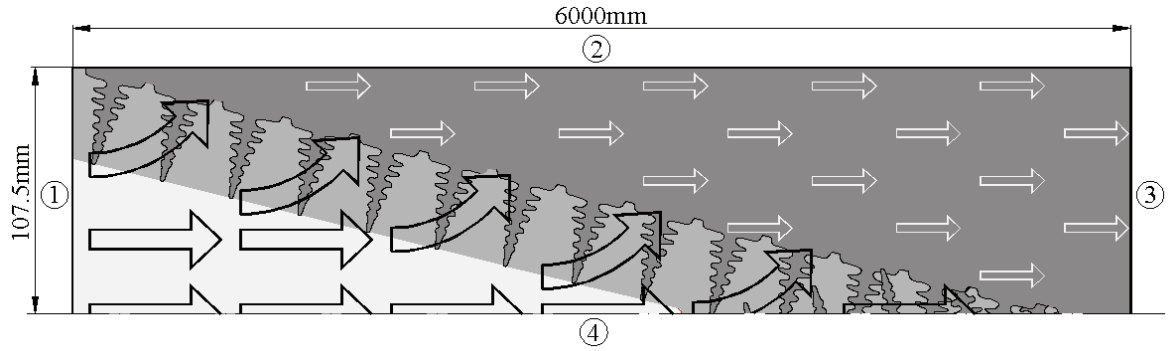

Fig. 3: Configuration of the calculation domain and boundary conditions (described in the text).

4. RESULTS AND DISCUSSION

The modeling results, graphically shown in this section, are presented in scaled figures with different scaling factors in the horizontal and vertical direction. Fig. 4a shows the temperature field (upper half) and volume fraction of the solid (lower half). Fig. 4b displays the liquid concentration c_l whereas Fig. 4c shows the mass transfer rate M_{lc}, Fig. 4d illustrates the surface term $f_{imp} \cdot A/V$ and finally Fig. 4e shows the average solid density ρ_s. In Fig. 5 the calculated Carbon macrosegregation field is displayed. Further details on that are given in Fig. 6, where macrosegregation profiles from the inlet, the outlet and across different sections are shown. For a comparison, Fig. 7 shows published macrosegregation profiles gained according to different macrosegregation forming mechanisms.

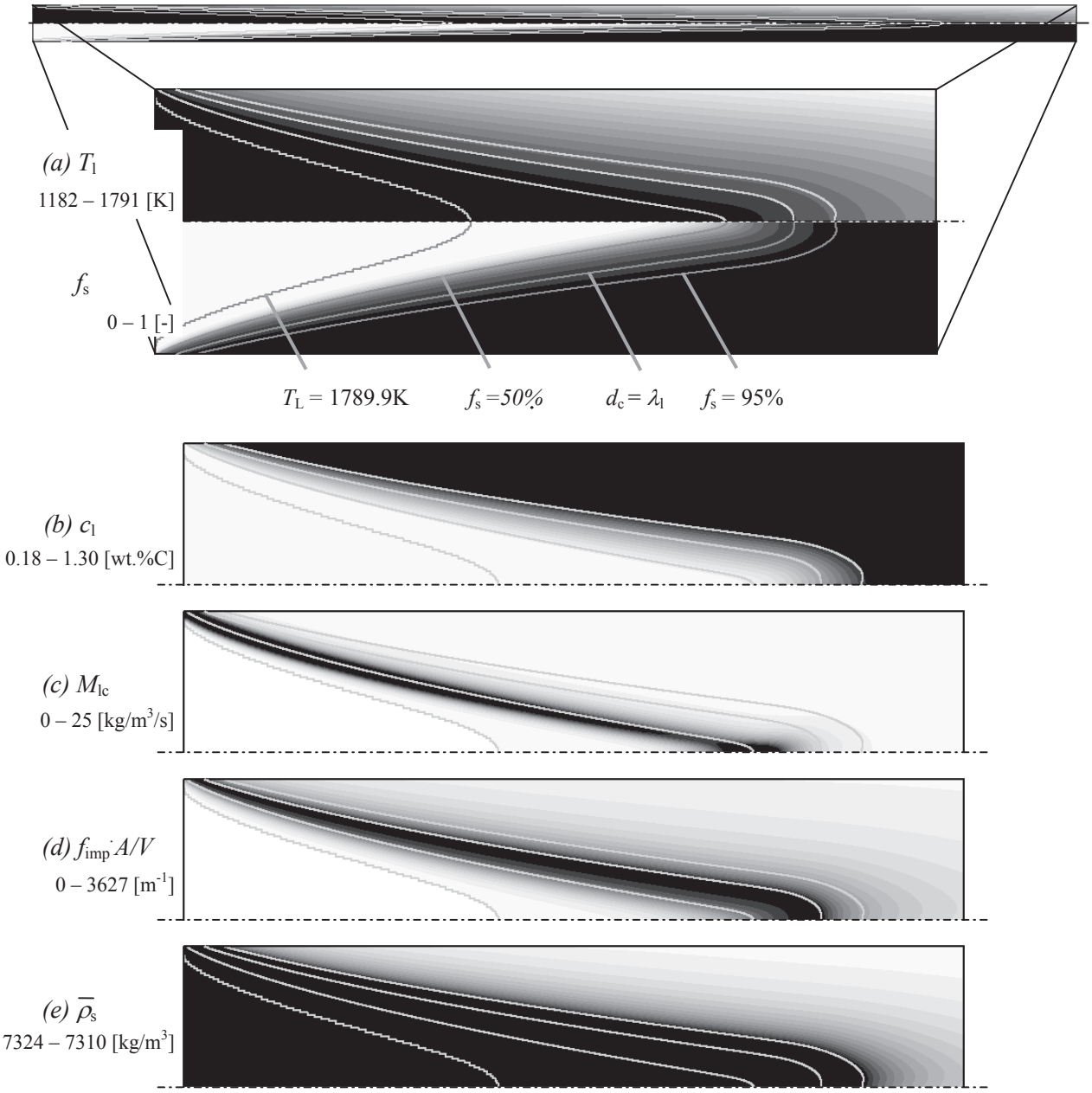

Fig. 4: (a) A scaled sketch of the temperature field (upper half) and volume fraction of the solid (lower half) of the continuous casting process for Fe-0.18 wt.%C, with (b) liquid concentration c_l, (c) mass transfer rate M_{lc}, (d) surface term $f_{imp} \cdot A/V$, and (e) average solid density $\overline{\rho}_s$. All fields are overlaid with different isolines as ladeled in Fig 4a. The bright areas represent the lowest values whereas the dark areas the highest.

In all figures the isotherm of the liquidus temperature T_L = 1789.9 K, where volume fraction of the solid is zero, f_s = 0, the isoline of f_s = 0.5 as well as the isoline of f_s = 0.95 and also the isoline of $d_c = \lambda_1$ is displayed. The mushy zone starts from T_L, and ends at the predefined liquid fraction limit of $f_l = 10^{-4}$. In order to avoid convergence problems hindered feeding, it was assumed that in the region of solid volume fraction larger than 0.95 pores might occur.

In a general solidification sequence, solidification starts at the cooled surface region as soon as the temperature drops below liquidus. According to the phase diagram informations the so formed solid has a smaller concentration than the melt and therefore the liquid starts to become enriched (see Fig. 4b). The difference between the averaged concentration within the cell and the equilibrium concentration at the phase boundary is responsible for the mass transfer rate M_{lc} (see Fig. 4c). With further cooling, the dendrite trunk diameter (d_c) grows whereby the surface per volume (A/V) increases. When d_c becomes larger than λ_1, the ap-

plied impingement factor (f_{imp}) leads to a reduction of the columnar growth surface area ($f_{imp} \cdot A/V$) so that the mass transfer tends to zero by consuming the residual melt. Fig. 4d shows that this product of f_{imp} and A/V has a maximum at the λ_1 - isoline. However, as shown in Fig. 4c, the maximum of the mass transfer rate is not at the λ_1 - isoline but rather at around the f_s = 0.5 - isoline. This indicates that the factor which is responsible for the maximum M_{lc} (according to 3) is the growth velocity v_{R_C} rather than the surface term $A/V \cdot f_{imp}$.

The proposed simplified-porosity-model starts to act at the predefined volume fraction of f_s = 0.95. This can be seen by the reduced average solid density $\overline{\rho_s}$ shown in Fig. 4e. As feeding is no longer necessary for solid volume fraction beyond 95%, we could avoid any major numerical convergence problem normally occurring when feeding flow starts to be more and more difficult. However, the choice of f_s = 0.95 as the starting point for porosity formation is somewhat artificial and not based on related physical phenomena. At presence, a corresponding improvement is under way. However, the present use of such a simplified-porosity-model ensures a stable numerical calculation right to any liquid fraction limit desired.

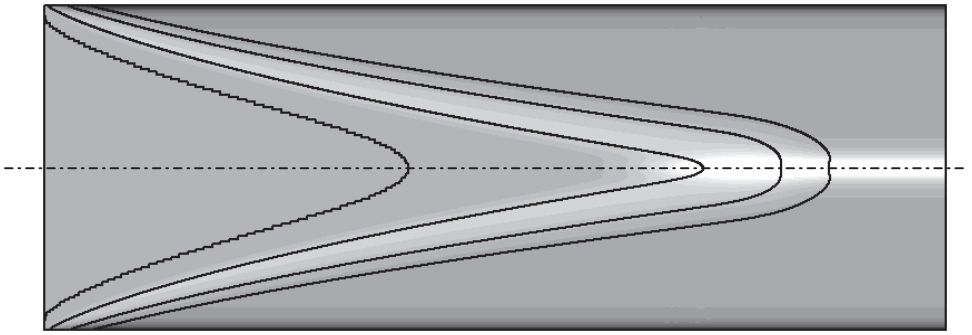

Fig. 5: Macrosegregation of C, isolines are defined as labelled in Fig. 4a. The range of the values is 0.176wt.%C (bright areas) - 0.184wt.%C (dark areas).

Fig. 5 shows the predicted macrosegregation pattern and Fig. 6 the corresponding macrosegregation developments at different positions along the length of the strand. As we consider the mush to be permeable, solidification-induced shrinkage flow occurs through the mushy zone up to the above mention predefine f_s = 0.95 limit. Since the early work of Flemings in 1967 [4], it is known that feeding flow towards the dendrites roots causes positive macrosegregation at the surface of a casting, the so-called inverse segregation. This is also observed in our simulations. In the center of the strand the solidifying dendrites are fed with less- or non-segregated 'fresh' melt coming from the bulk region in the middle of the casting. Therefore, the solid there is formed with a decreased solute content and negative macrosegregations occur at the center line.

Contradicting to this result, positive centerline macrosegregation is often reported in practice. Based on our study, the explanation of positive centerline segregation has to consider additional phenomena, such as bulging or bending. Fig. 7 shows a comparison of calculated macrosegregation profiles with and without bulging or shrinkage (taken from [5]). Our result coincides with these results, as negative center segregation is predicted when only shrinkage flow is considered. The two other lines, namely the broken line and the continuous line in Fig. 7, show the positive centerline segregation results induced by bulging with/without shrinkage. It indicates that in the general case, positive centerline segregation would be expected when bulging is important. The difference in the profiles in Fig. 6 and Fig. 7, especially far away from the center, depends on the different boundary conditions of the simulations. However industrial practice also shows that in some special cases, for example in large round billet castings especially for non-ferrous materials where bulging is of minor importance, negative centerline segregation exists.

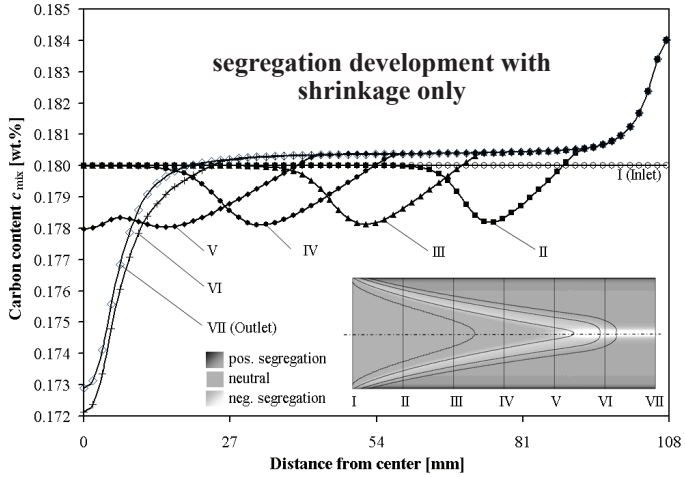

Fig. 6: Macrosegregation pattern at the inlet, the outlet and different cross section positions.

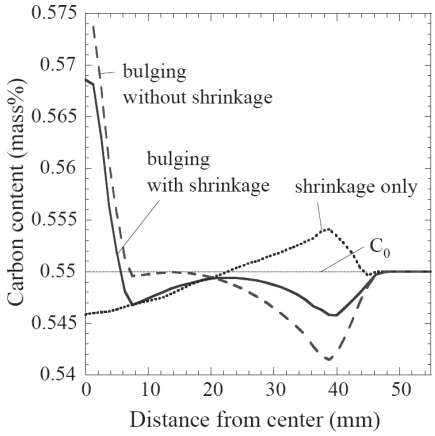

Fig. 7: Carbon profile across the strand for different macrosegregation forming mechanisms according to [5].

5. CONCLUSIONS

A two phase Eulerian approach is used to model the shrinkage flow induced macrosegregations in steel continuous casting. The presented model includes an implementation of a hexagonal staggered columnar growth model combined with a simplified porosity model. The results show positive macrosegregations at the wall and negative ones in the center line. These results confirm the previous studies in literature. Negative centerline segregation is often experimentally observed in round billets, although positive centerline segregation is normally found for steel slabs in industry. According to Miyazawa [1] and Kajitani [5], this positive segregation is mainly due to bulging. The inclusion of bulging and other macrosegregation formation mechanisms in the Eulerian approach is the objective of further studies.

6. ACKNOWLEDGEMENT

This work is financially supported by the Austrian Christian-Doppler Research Society, voestalpine Stahl Donawitz, voestalpine Stahl Linz and Siemens VAI Metal Technologies for which the authors kindly acknowledge. The authors wish to express their appreciation to ANSYS Inc./FLUENT Inc. for their technical assistance.

7. REFERENCES

[1] K. Miyazawa, K. Schwerdtfeger, Arch. Eisenhüttenwesen, 52 (1981) 415.

[2] C. Beckermann, Int. Mater. Rev., 47 (2002) 243.

[3] G. Lesoult, Mater. Sci. Eng. A., 413-414 (2005) 19.

[4] M.C. Flemings, ISIJ Intern., 40 (2000) 833.

[5] T. Kajitani, J.-M. Drezet, M. Rappaz, Met. Mater. Trans., 32A (2001) 1479.

[6] S. Ogibayashi, M. Kobayashi, M. Yamada, T. Mukai, ISIJ Intern., 31 (1991) 1400.

[7] C.H. Yin, J.K. Park, B. D. You, S.M. Yang, ISIJ Intern., 36 (1996) 231.

[8] R. Thomas, K. Harste, Steel Res., 75 (2004) 693.

[9] H. Preßlinger, S. Ilie, P. Reisinger, A. Schiefermüller, A. Pissenberger, E. Parteder, S. Bernhard, ISIJ Intern., 46 (2006) 1845.

[10] S.Y. Lee, A.I. Chung, A.P. Hong, McWASP IX, SIM2000, ed. P. Sahm, P.N. Hansen, G. Conley, (2000) 648.

[11] A. Ludwig, M. Wu, Mater. Sci. Eng. A, 413-414 (2005) 109.

[12] M. Wu, A. Ludwig, Metall. Mater. Trans., 37A (2006) 1613.

[13] Bird R.B., Steward W.E., Lightfoot E.N., "Transport Phenomena", John Wiley & Sons, New York (1960).

[14] A. Ludwig, M. Wu, Metall. Mater. Trans., 33A, (2002) 3673.